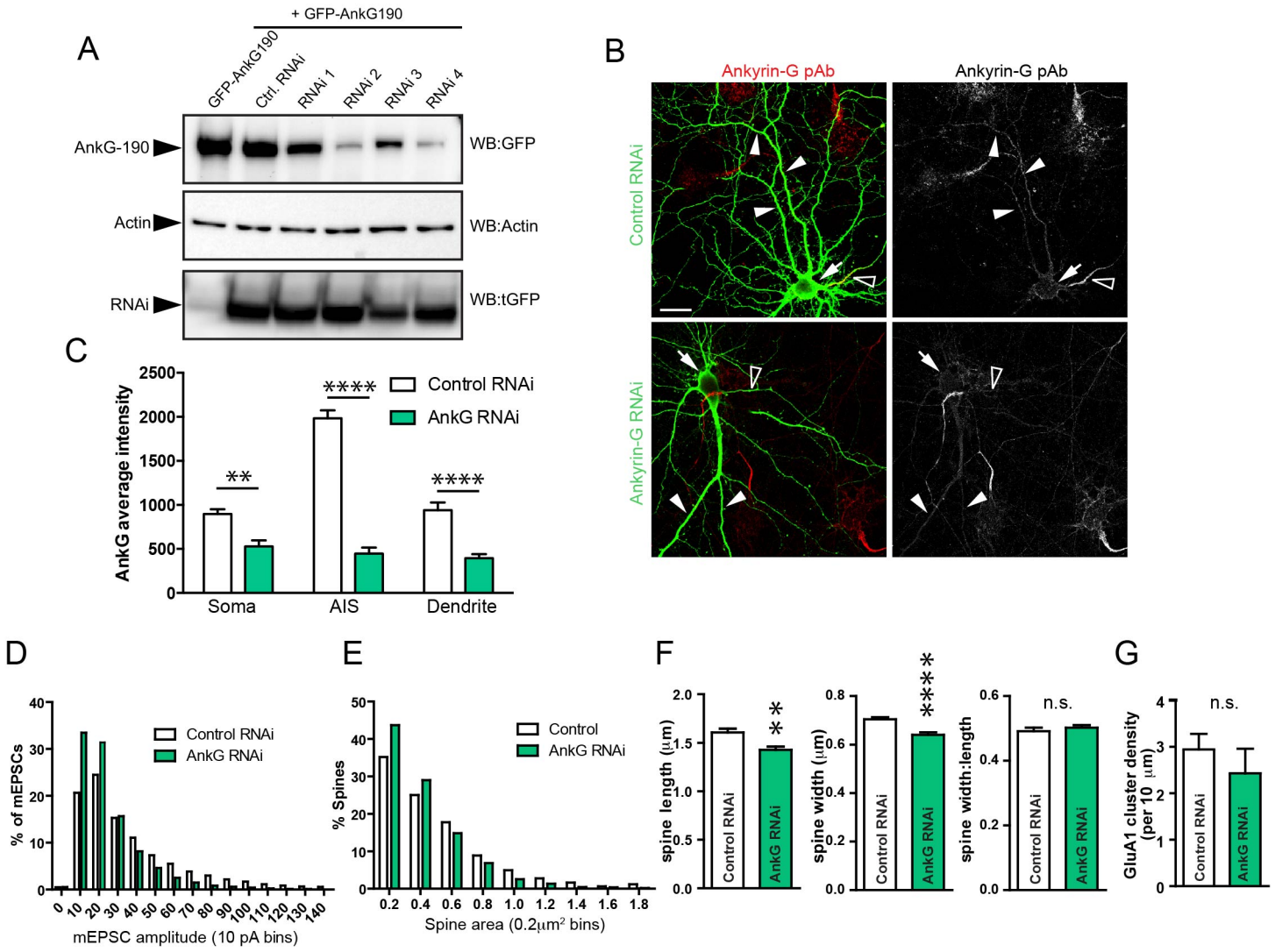

Figure S1, related to Figure 1; Characterization of ankyrin-G RNAi

A. Knock-down of ankyrin-G-190-GFP in HEK cells. SDS-PAGE and western blot of lysates from HEK cells expressing ankyrin-G-190-GFP alone or with control or candidate RNAi constructs. RNAi construct 4 was utilized for all experiments.

B. Confocal images of neurons expressing control or ankyrin-G RNAi and immunostained with antibodies to ankyrin-G, scale bar=20μm.

C. Summary bar graph comparing intensities of ankyrin-G fluorescence in the soma, axon initial segment (AIS) and dendritic compartments of cortical neurons expressing control or ankyrin-G RNAi constructs. ****p<0.0001, soma **p<0.01, AIS ****p<0.0001,dendrite ****p<0.0001, n=11-12 cells. D. Frequency histogram of mEPSC event amplitudes.

E. Frequency histogram of dendritic spine areas.

F. Additional measurements of spine morphology and density for ankyrin-G knock-down experiments. Spine length: **p=0.0015, spine width: ****p<0.0001, spine width:length: p=0.412, n=16-18 cells.

G. Quantification of GluA1 cluster density in control and ankyrin-G knockdown neurons (p=0.262, n=11-14 cells)

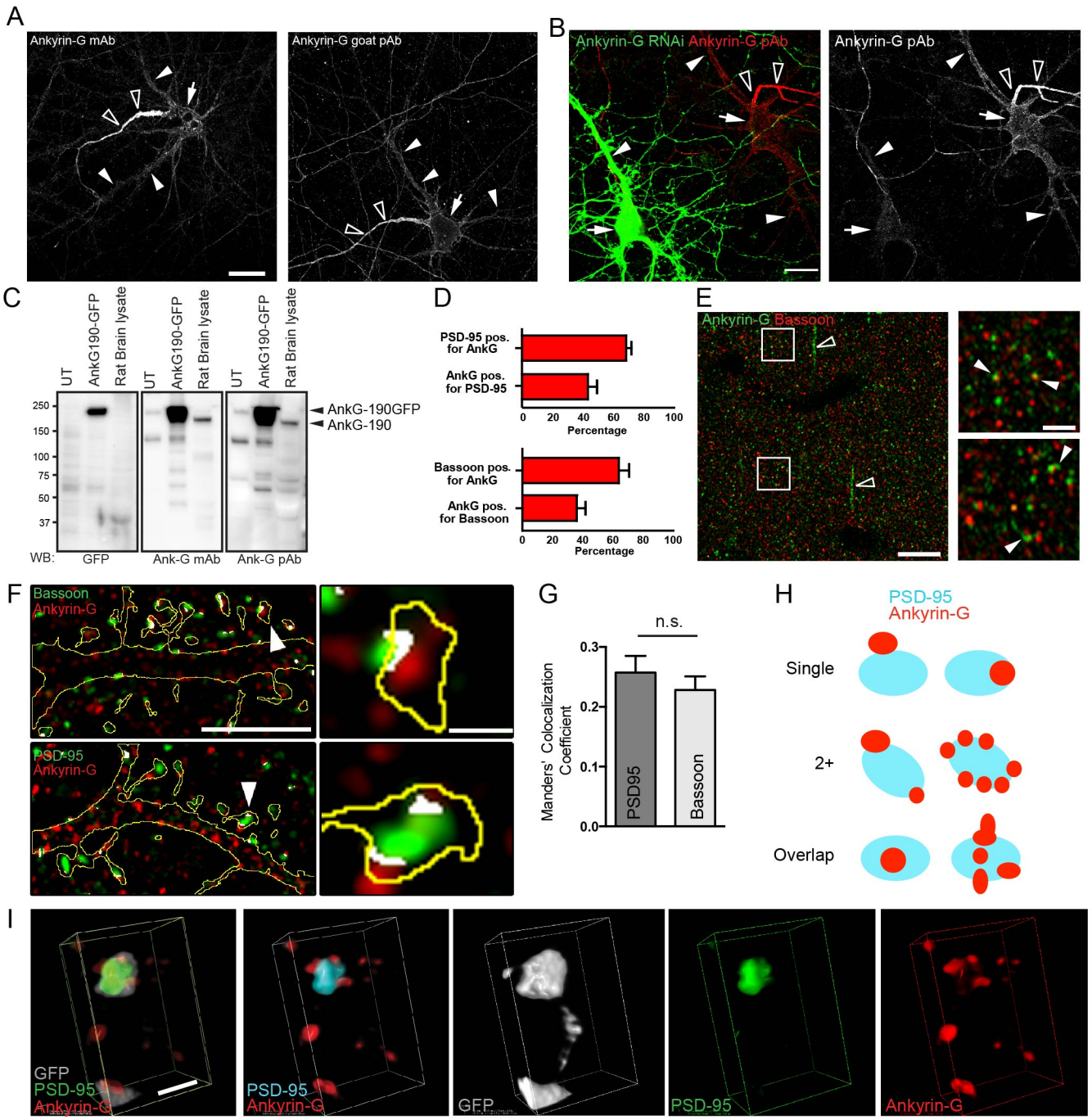

Figure S2, related to Figure 2; Ankyrin-G endogenous labeling experiments

A. Confocal images of cortical neurons immunostained with 2 other antibodies to ankyrin-G (ankyrin-G monoclonal (mAb) and goat polyclonal (pAb)) showing similar distributions at the AIS and in dendrites. Scale bar=20 µm.

B. Confocal image of neuron transfected with ankyrin-G RNAi and neighboring untransfected neuron showing lack of ankyrin-G labelling in the transfected neuron.

C. SDS-PAGE and western blot of lysates from HEK 293 cells either expressing Ankyrin-G-190-GFP or untransfected (UT) and rat brain lysate. Blots are probed with antibodies to GFP, ankyrin-G mAb, or ankyrin-G rabbit pAb.

D. Colocalization analysis of confocal imaging in Figure 2B-D showing overlap between ankyrin-G puncta and PSD-95 and bassoon puncta (n= 5 cells per condition).

E. Confocal image of cortical brain slice immunostained for ankyrin-G (green) and bassoon (red) showing localisation of ankyrin-G at the AIS (open arrowheads) and at synapses (closed arrow heads). Scale bar=10 µm, 2µm.

F. SIM images of neurons labelled with antibodies to ankyrin-G (red) and either bassoon or PSD95 (green). White regions show areas of colocalization as determined by the colocalization tool. Scale bars = 2 µm and 0.5 µm

G. Summary bar-graph of Manders' colocalization coefficient for ankyrin-G overlap with either PSD-95 or bassoon (p=0.443, n=5 cells, n.s.=non-significant).

H. Schematic showing examples of distribution of ankyrin-G nanodomains with respect to PSD-95.

I. 3D-reconstruction of GFP-filled spine labeled with antibodies to ankyrin-G and PSD-95. Scale bar= 0.5 µm.

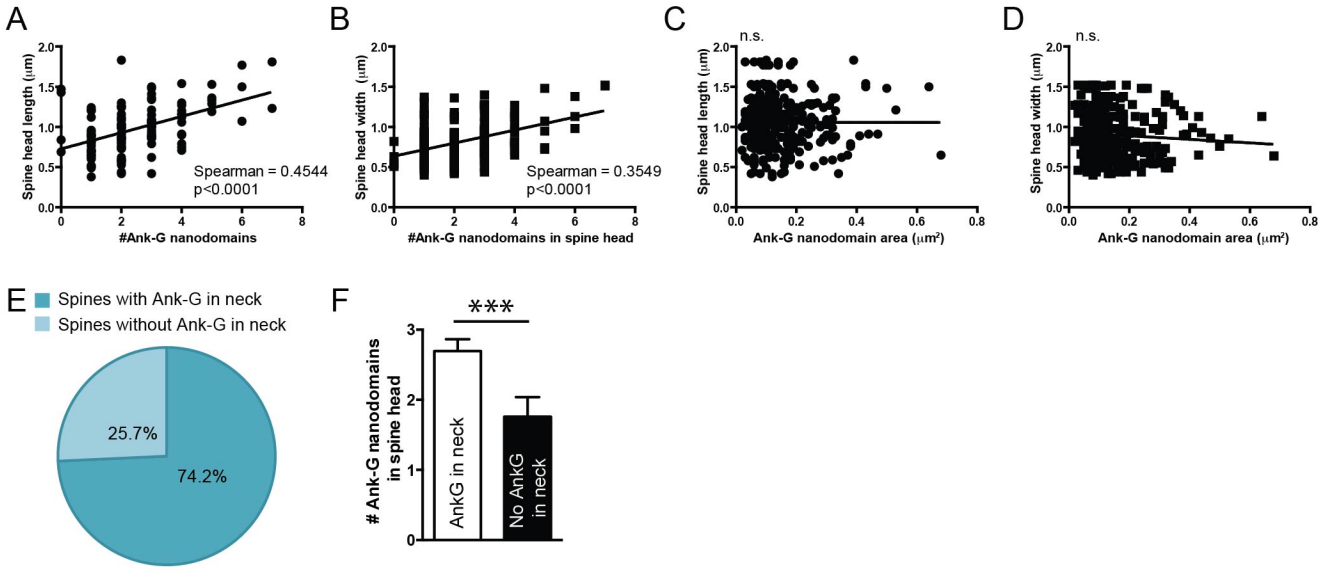

Figure S3, related to Figure 3; Further analysis of ankyrin-G nanodomains in dendritic spines

A. Correlation of spine head length with the number of ankyrin-G nanodomains in the spine head ($p<0.0001$, spearman=0.454). B. Correlation of spine head width with the number of ankyrin-G nanodomains in the spine head ($p<0.0001$, spearman=0.354). C. Correlation of spine head length with ankyrin-G nanodomain area ($p=0.952$, spearman=-0.003). D. Correlation of spine head width with ankyrin-G nanodomain area ($p=0.059$, spearman=-0.109, n=299 nanodomains). E. Pie chart showing 74.2% of dendritic spines have ankyrin-G nanodomains in the spine neck. F. Summary bar graph of the number of ankyrin-G nanodomains in the spine heads of spines with or without ankyrin-G in the neck, (***$p=0.0009$).

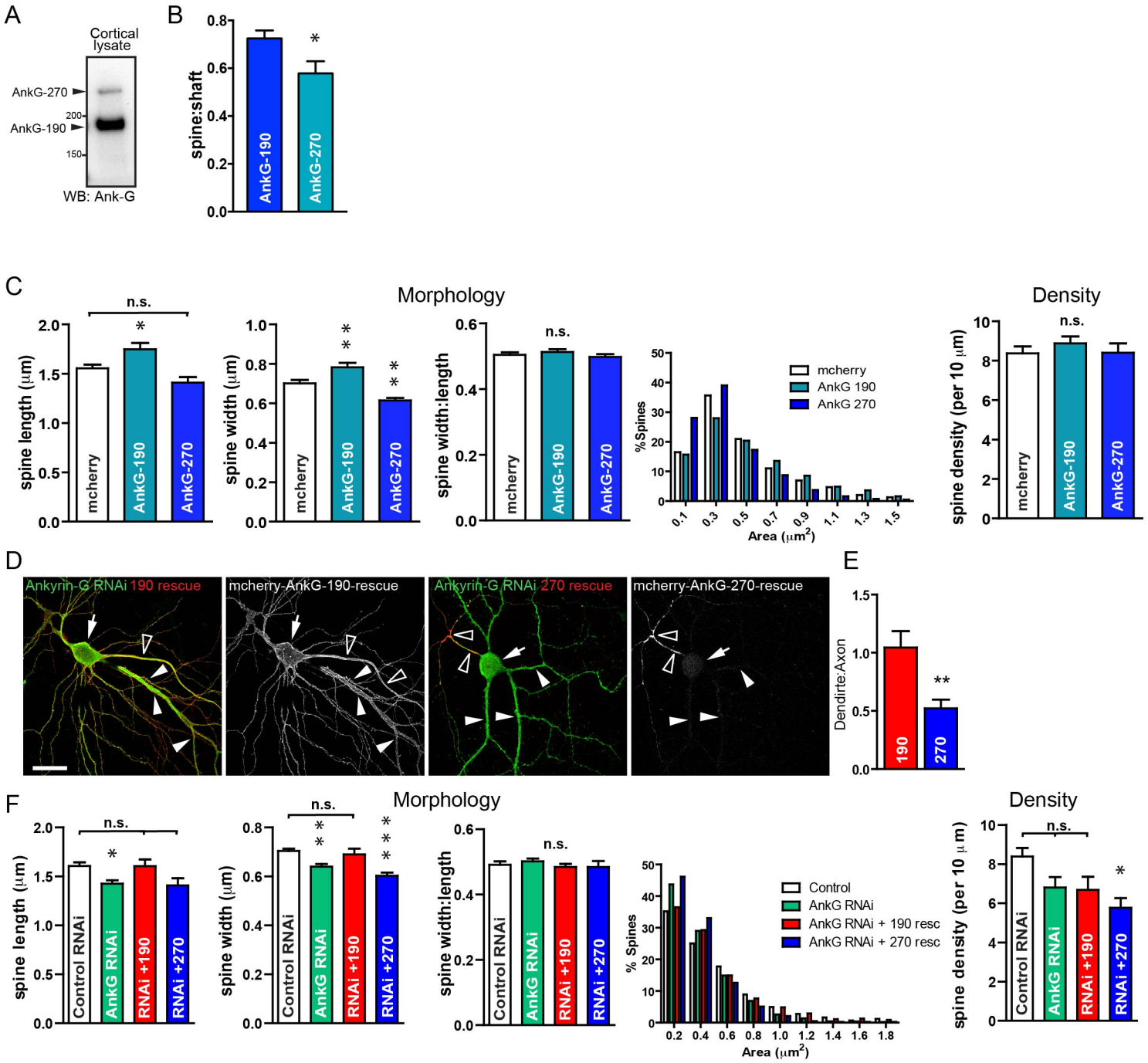

Figure S4, related to Figure 4; Ankyrin-G isoform control experiments

A. SDS-PAGE and western blot of rat cortical lysate probed with antibodies to ankyrin-G showing the abundance of the 190 kD isoform in the cortex.

B. Bar graph summarizing spine:shaft for GFPAnkG190 or GFPAnkG270 constructs, p=0.02.

C. Additional measurements of spine morphology and density for ankyrin-G overexpression experiments. Spine length: p=0.0002, spine width: p<0.0001, spine width:length: p=0.476.

D. Confocal images of control and knockdown neurons coexpressing mcherryAnkG190 and mcherryAnkG270 RNAi resistant constructs. RNAi resistant AnkG190 localises to dendrite and axon equally, whereas RNAi resistant AnkG270 localises primarily to the axon (E).

F. Additional measurements of spine morphology and density for ankyrin-G RNAi rescue experiments. Spine length: p<0.05, spine width: p<0.05, spine width:length: p=0.294, spine density: p=0.016.

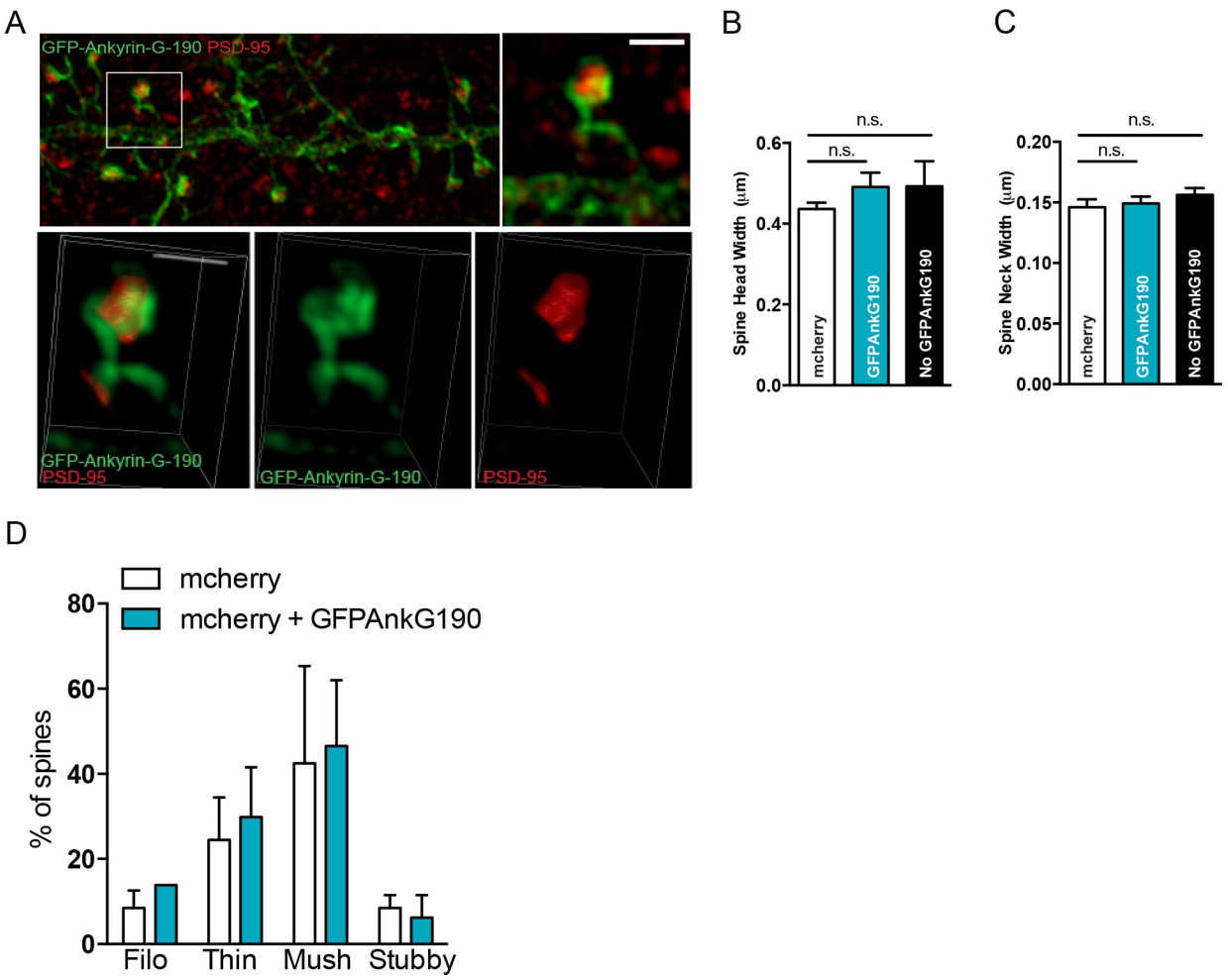

Figure S5, related to Figure 5; Additional Ankyrin-G 190kD SIM experiments

A. SIM image of cortical neuron expressing GFP-Ankyrin-G-190 and stained with antibodies to PSD-95. 3D-reconstruction of spine showing the 190 kD isoform of ankyrin-G is perisynaptic forming around the PSD. Scale bars=0.5μm.

B,C. Bar graphs summarizing spine head width and neck width in thin spines from mcherry control cells and GFPAnkG190 overexpressing cells (p=0.416, p=0.533).

D. Bar graph summarizing analysis of spine subtypes in neurons expressing mcherry + GFPAnkG190 or mcherry alone.

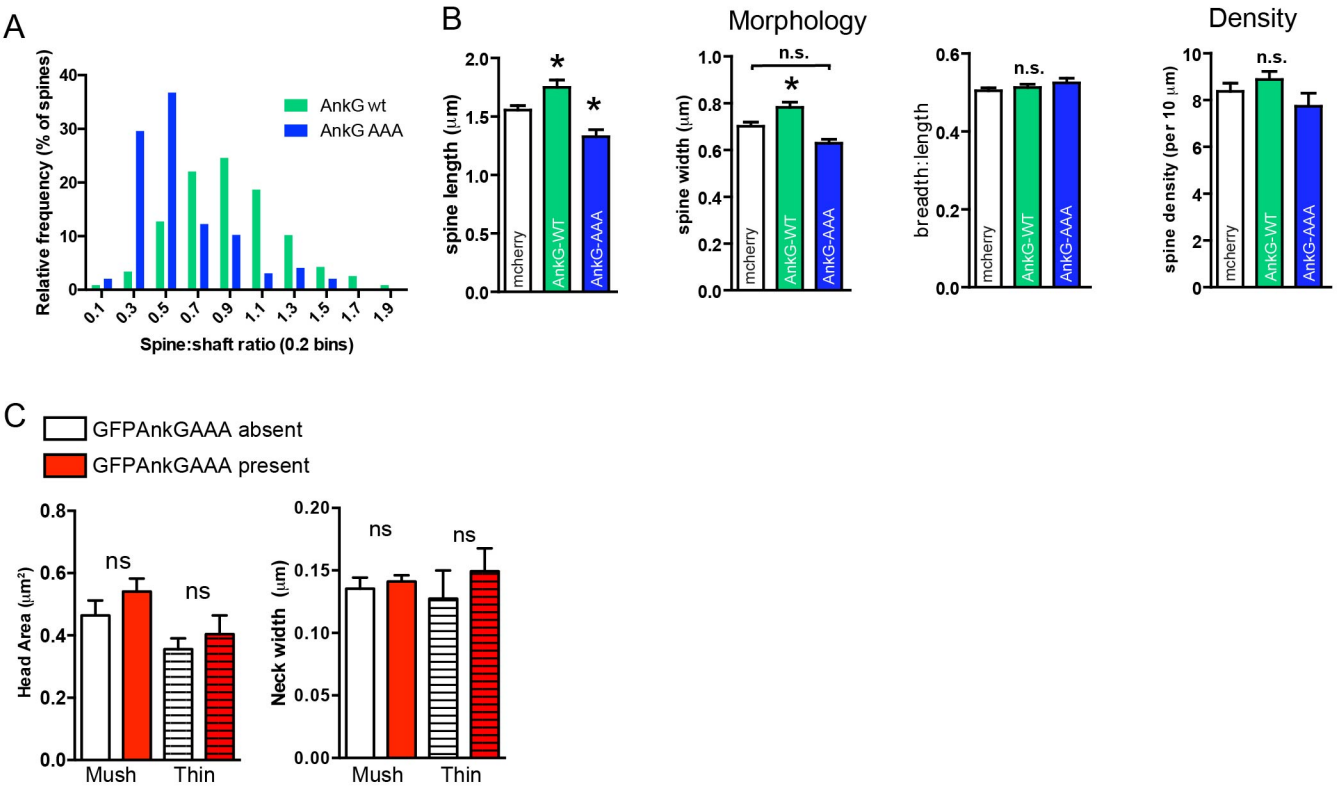

Figure S6, related to Figure 6; Spine morphology data for GFPAnkGAAA mutant expression
A. Frequency distribution graph of spine:shaft ratios for GFPAnkG190 and GFPAnkGAAA, from confocal images.
B. Additional measurements of spine morphology and density for ankyrin-G mutant confocal imaging experiments. Spine length: $p<0.0001$, spine width: $p<0.0001$, spine width:length: $p=0.314$, spine density: $p=0.193$. n.s.=non-significant.
C. Analysis of spine geometry from SIM images of neurons expressing the GFPAnkGAAA mutant. Overexpression of GFPAnkGAAA in head and neck causes no change in spine head area or neck width (compare to overexpression of GFPANkG190, Figure 5F).
Data are mean ± SEM.

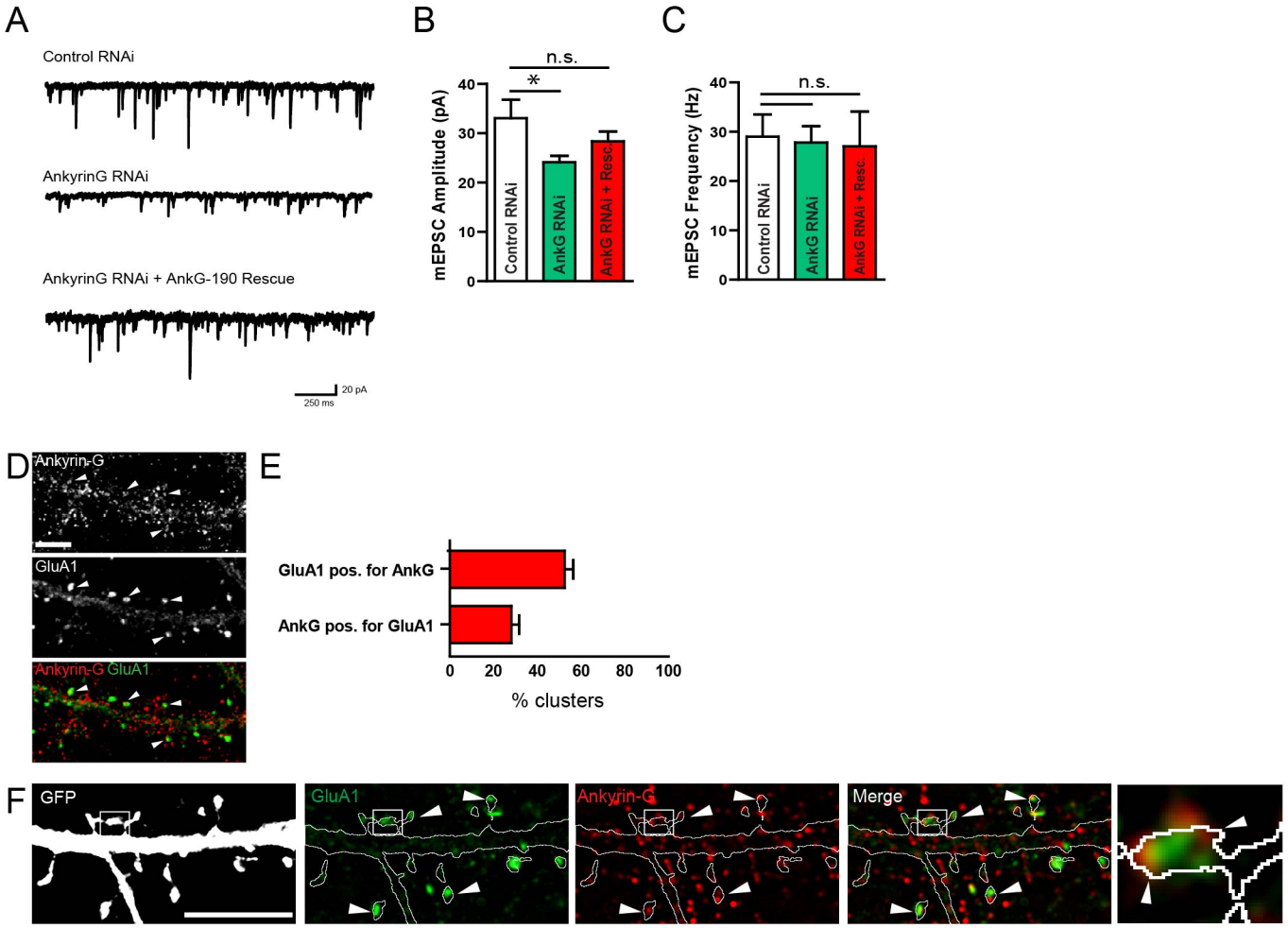

Figure S7, related to Figure 7; Ankyrin-G localization with GluA1

A. Representative mEPSC recordings from neurons expressing control RNAi, ankyrin-G RNAi or ankyrin-G RNAi + RNAi resistant GFPAnkG190. Data for control and ankyrin-G RNAi are as in Figure 1.

B. Bar graphs of mEPSC amplitude and frequency.

D. Confocal images of cortical neuron immunostained for ankyrin-G and GluA1. Scale bar=5μm.

E. Quantification of colocalization between ankyrin-G and GluA1 clusters from confocal images (n=12 cells).

F. SIM image of neuron immunostained for ankyrin-G and GluA1. Scale bar= 5μm.

Data are mean ± SEM.

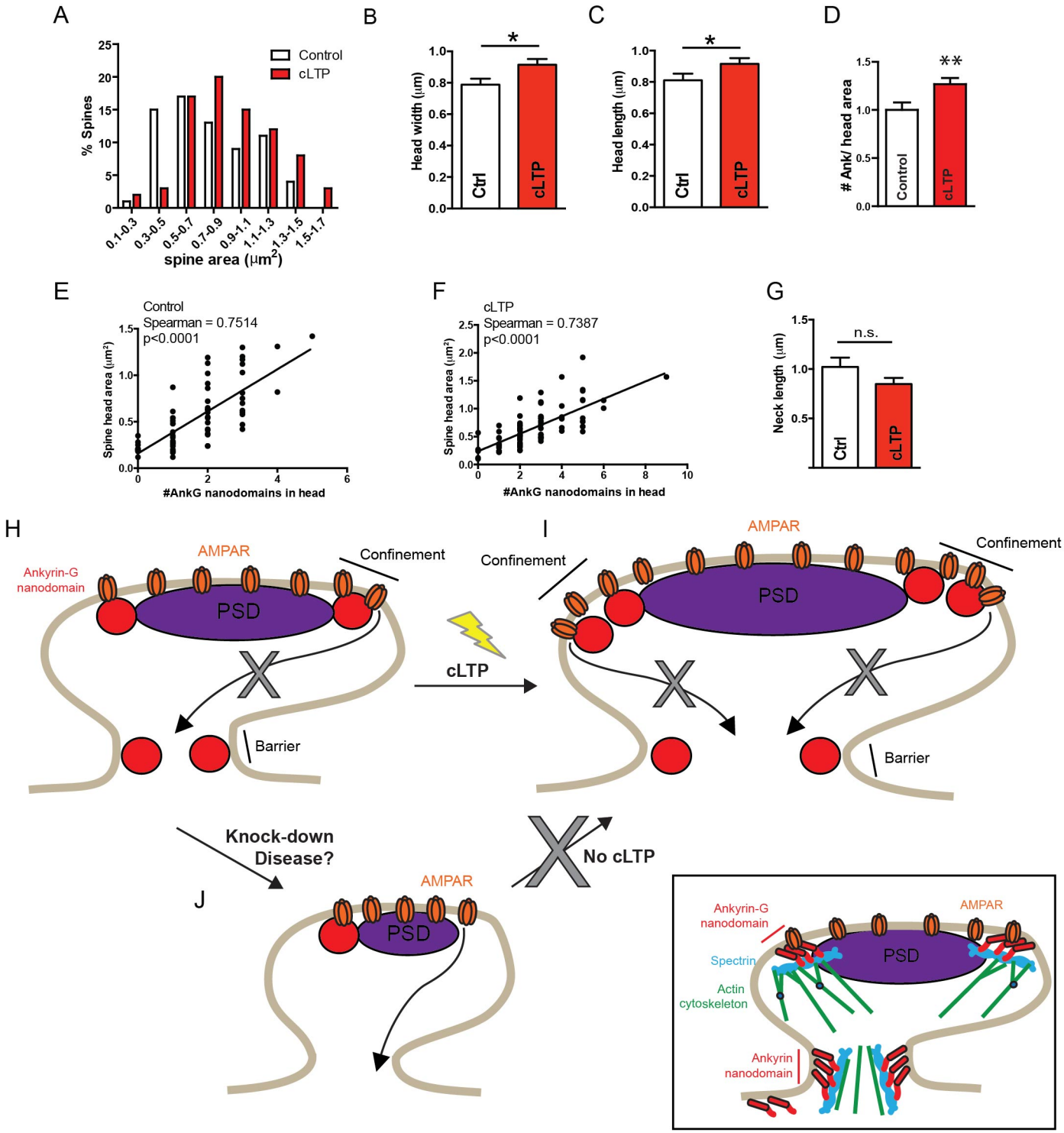

Figure S8, Related to Figure 8; Additional spine measurements from SIM imaging and summary

A-G. Additional measurements of spines from SIM images of control or cLTP treated GFP expressing neurons. A.Frequency histogram of spine head area for control and cLTP neurons from SIM images. B. Summary bar graph of spine head width in control and cLTP conditions (p=0.018,t-test) . C. Summary bar graph of spine head length in control and cLTP conditions (p=0.047, t-test). D. Summary bar graph of spine neck length in control and cLTP conditions (p=0.303). D. n=69-81 spines per condition.

E,F. Correlations of spine head area and ankyrin-G nanodomain number in control (E) and cLTP (F) conditions.

G. Normalized ankyrin-G nanodomain number in control and cLTP conditions (**p<0.001, n=67-70 spines).

H-J. Schematic summarizing the localization and function of ankyrin-G in dendritic spines. H. In dendritic spines ankyrin-G forms nanodomains (red) at perisynaptic sites and within the spine neck. Ankyrin-G nanodomains function to confine AMPARs (orange) to the spine head. Binding to spectrin (blue) is required for both targeting of ankyrin-G and its function in maintaining spine structure. I. Neuronal activity causes increased nanodomain number in the dendritic spine head. J. Knock-down of ankyrin-G causes decreased spine area and synaptic transmisson, and makes spines resistant to cLTP-dependent spine enlargement.

Extended Experimental Procedures

Plasmids and antibodies

GFP-Ankyrin-G-190 and RFP-Ankyrin-G-270 were purchased from Addgene (#31059, #42566). RNAi constructs were purchased from Origene, in the pGFP-V-RS vector with a turboGFP element to enable identification of transfected cells. The target sequence used was GGCAGAACGAGACGCCAAGTGGAAGCCTA. RNAi resistant GFP-Ankyrin-G-190/270 and Spectrin-binding mutant construct (Kizhatil et al., 2007) were generated using QuickChange Site-Directed Mutagenesis Kit (Stratagene). Three non-coding mutations were incorporated into the RNAi target sequence to generate the RNAi-resistant Ankyrin-G constructs. All constructs were sequence verified. pEGFP-N2 and pmCherry-C1 (Clontech) were overexpressed in cultured neurons for morphometric analysis experiments. GluA1-SEP was a gift from Richard Huganir. The following primary antibodies were used: Ankyrin-G mAb (Neuromab), PSD95, (Neuromab), Ankyrin-G pAb (Santa Cruz), Ankyrin-G pAb (from V. Bennett), Spectrin pAb (AbCam), Bassoon (Assign Technologies), GluA1 (Millipore), turboGFP mAb (to identify RNAi expression, Origene), DsRed pAb (to identify mcherry expression, Clontech), GFP chicken pAb GFP (to identify GFP expression, Abcam).

Statistical analysis

All statistical tests were performed with GraphPad Prism. Data were tested for normality with D'Agostino and Pearson to determine use of non-parametric (Mann-Whitney, Kruskal-Wallis, Spearman correlations), or parametric (unpaired t-test, ANOVA, Pearson's correlations) tests. Post-hoc tests were included in analyses with multiple comparisons. Bar graphs are displayed as mean ± SEM, unless otherwise noted. P

values were considered significant if < 0.05. N numbers refer to number of cells per condition unless otherwise stated.

SIM imaging and analysis

Imaging and reconstruction parameters were empirically determined with the assistance of the expertise in the Nikon Imaging Center at Northwestern, with the best image in mind. Acquisition was set to 10MHz, 14 bit with EM gain and no binning. Auto exposure was kept between 100-300ms and the EM gain multiplier restrained below 300. Conversion gain was held at 1x unless necessary to increase signal with 2.4x. Laser power was adjusted to keep LUTs within the first quarter of the scale (<4000). Three reconstruction parameters (Illumination Modulation Contrast, High Resolution Noise Suppression and Out of Focus Blur Suppression) were extensively tested to generate consistent images across experiments without abnormal features or artifacts and producing the best Fourier transforms. Reconstruction parameters (0.96, 1.19, and 0.17) were kept consistent across experiments and imaging sessions. Resolution of images was confirmed with full-width half maximum (FWHM) measurements of a small structure within the image. The remarkable similarity of measurements of spines in these images and those from both STED and EM (where no reconstruction parameters are needed) lends validity to the settings chosen.

For each spine analyzed, the single plane in which the neck of the spine or the spine head were in focus, based on the cell fill, was chosen for analysis (could be different planes for neck and head). Using the Nikon Elements software, each spine head and neck were outlined manually in the channel of the cell fill to detect the area. Classification of spine type was done based on apparent morphology and traditional classification schemes (Amatrudo et al., 2012). Spine head height and width were

assessed as the widest points parallel to and perpendicular to the long axis of the spine neck. Spine neck length was manually measured from dendritic shaft to base of spine head (long axis of spine neck). Spine neck width was assessed as the full width half-maximum (FWHM) and was measured in ImageJ with a linescan across the maximum width of the neck. Gaussian fits of these intensity profiles were performed in GraphPad Prism and the FWHM was calculated. PSD, GluA1, Bassoon and ankyrin-G puncta within the spine head were manually outlined and the area recorded. Visual assessment of fluorescence intensity was used to delineate separate or connected puncta. Puncta were considered separate if a region of decreased intensity was readily visible. This approach was confirmed with the NIS Elements automated detection software and kept consistent throughout all SIM analyses. Measurement of the relative distances between the centers of the puncta (e.g. Ankyrin to PSD) was drawn manually. The number of puncta within the spine head was quantified manually and recorded. Based on the localization of Ankyrin-G within the spine head, in relation to the postsynaptic marker (PSD or GluA1), dendritic spines were classified into one of three groups. The 1 ANK group included spines with only one puncta of Ankyrin-G nearby (adjacent-to or just within the edge of the PSD or GluA1 puncta). The 2+ ANK group contained all dendritic spine heads containing two or more Ankyrin-G within or near the PSD or GluA1 as long as those Ankyrin-G puncta within the PSD or GluA1 were confined to the edges. The Overlap group contained spines in which Ankyrin-G puncta were entirely enveloped within the PSD or GluA1, with close to 100% colocalization. Whether or not Ankyrin-G was present within the spine neck was assessed based on the presence or absence of fluorescent signal within the confines of the GFP-derived spine neck outline. Ratiometric images were produced in MetaMorph with cell fill serving as the denominator. Colocalization highlighter images and Manders' colocalization coefficients were determined in ImageJ, after thresholding, with the use of the MBF set of plugins. Three-

dimensional reconstructions of dendritic spines were created in the Nikon Elements Software by merging a dimmed maximum projection of the GFP signal with shaded volume reconstructions of the two other channels, to allow for better visualization.

Neuronal cell culture and transfection

Dissociated cultures of primary cortical neurons were prepared from E18 Sprague-Dawley rat embryos. Brains were dissected in ice-cold Hank's buffered salt solution, and cortical tissue isolated, digested with papain (Sigma; diluted in Neurobasal with EDTA (0.5 mM) and DNaseI (2 units/mL), activated with L-cysteine (1 mM) at 37°C), and mechanically dissociated in neuronal feeding media (Neurobasal + B27 supplement, Invitrogen + 0.5 mM glutamine + penicillin/streptomycin). 1hr after feeding, media was replaced. Neuronal cultures were maintained at 37°C in 5% CO_2. Neuronal feeding media was supplemented with 200 µM D,L-amino-phosphonovalerate (D,L-APV, Ascent Scientific) beginning on DIV 4. Neurons were transfected at DIV21 with Lipofectamine 2000, providing a transfection efficiency of 0.5-1%. Plasmids (1-10 µg total DNA) and Lipofectamine 2000 (Invitrogen) were diluted in Dulbecco's Modified Eagle Medium (DMEM) + HEPES (10 mM), mixed thoroughly together, and incubated for 20-30 minutes at 37°C before adding to cultured cells. Following transfection, neurons were supplanted in antibiotic-containing feeding media containing half conditioned and half fresh media, and allowed to express constructs for 3 days or as indicated.

Immunocytochemistry

Cells were fixed for 10 min in 4% formaldehyde/4% sucrose in PBS and then 4°C in methanol pre-chilled to -20°C for 10 min. Fixed neurons were permeabilized and blocked simultaneously in PBS containing 2% normal goat serum and 0.2% Triton-X-100 for 1 hr at room temperature. Primary antibodies were added in PBS containing 2% normal goat

serum overnight at 4 °C, followed by 3 x 10 min washes in PBS. Secondary antibodies were incubated for 1 hr at room temp, also in 2% normal goat serum in PBS. Three further washes (15 min each) were performed before coverslips were mounted using ProLong antifade reagent (Life Technologies).

Pharmacological treatments

Chemical LTP experiments were performed as previously described (Xie et al., 2007). Neurons were preincubated in ACSF (in mM: 125 NaCl, 2.5 KCl, 26.2 $NaHCO_3$, 1 NaH_2PO_4, 11 glucose, 5 HEPES, 2.5 $CaCl_2$ and 1.25 $MgCl_2$) with 200 µM APV for 30 min at 37°C. Coverslips were then washed in ACSF and transferred into treatment medium for 30 minutes (ACSF without $MgCl_2$, plus 10 µM glycine, 100 µm picrotoxin, and 1 µM strychnine). Neurons were then fixed and processed as described above.

Confocal microscopy

Confocal images of immunostained neurons were obtained with a Ziess LSM5 Pascal confocal microscope. Images of neurons were taken using the 63x oil-immersion objective (NA = 1.4) as z-series of 5-10 images, averaged 2 times, taken at 0.37 µm intervals, with 1024x1024 pixel resolution. Detector gain and offset were adjusted in the channel of cell fill (GFP or mcherry) to include all spines and enhance edge detection.

Confocal image analysis

Colocalization of synaptic proteins (Bassoon, PSD95 and GluA1) with ankyrin-G was quantified using MetaMorph. Background-subtracted images were thresholded, regions along dendrites were outlined, and total immunofluorescence intensity for each cluster was measured automatically. To determine the degree of colocalization between two channels, each channel was thresholded to select distinct puncta as described above. A 100µm dendritic region was selected and puncta counts were made; puncta smaller than

0.065 μm^2 were excluded from analysis. Regions representing the measured puncta in one channel were generated using Metamorph and overlayed on the other channel. Puncta were counted as colocalized if the average intensity within the overlaid region exceeded threshold. Thresholds were set individually for each antibody and held constant across treatment condition.

To determine spine protein content, spine regions generated by spine dimension analysis in MetaMorph were overlaid onto the appropriate channel and intensities within the spine regions were recorded. Dendritic shaft values were calculated as the mean intensity of 3 regions of shaft along the analysed dendritic region and used with corresponding spine values to produce spine:shaft ratios.

Linescans were performed in ImageJ (National Institutes of Health *hhtp://rsbweb.nih.gov/ij*). For ankyrin-G mutant analysis a 4μm linescan was performed across 3-5 spines per neuron and averaged across neurons to produce average linescans ± SEM.

Dendritic spine quantification

Two-dimensional, background-subtracted maximum projection reconstructions of images for dendritic spine morphometric analysis (area, length, and width), and quantification of spine linear density (# of spines/10 μm dendritic length) were performed using MetaMorph software (Molecular Devices). A threshold was applied to the maximum projection images to include all detectable spines, and regions along dendrites containing dendritic spines were manually traced to enclose spines but not dendritic shaft or other structures. Dendritic spine "objects", restricted to objects with areas greater than 0.1 μm^2, were automatically detected by MetaMorph, and the area, maximum length and head width of each spine was measured. Two dendritic branches

(approximately 100 µm) of each neuron were analyzed. Only spines on secondary and tertiary apical dendrites were measured to reduce variability. Cultures that were directly compared were stained simultaneously and imaged with the same acquisition parameters. For each condition, 3-10 neurons each from 2-5 separate experiments were used. Experiments were performed blind to conditions and on sister cultures.

Electrophysiology

Cultured cortical neurons were recorded in whole-cell configuration 3-4 days post-transfection (DIV24-25). The extracellular solution contained 140 mM NaCl, 10 mM glucose, 10 mM HEPES, 3 mM KCl, 2 mM CaCl2, 1 mM MgCl2 (pH 7.3). Patch pipettes were pulled from borosilicate glass and fire-polished to a resistance of 3–5 MΩ. The intracellular patch- pipette solution contained 95 mM CsF, 25 mM CsCl, 10 mM HEPES, 10 mM EGTA, 2 mM NaCl, 2 mM Mg-ATP, 10 mM QX-314, 5 mM tetraethylammonium chloride, 5 mM 4-amino- pyridine (pH 7.2). Neurons were voltage-clamped at -70 mV, and currents were recorded using pClamp9 software with an Axopatch 200B amplifier (Molecular Devices). mEPSCs were isolated by bath application of 10 µM bicucculine, 50 µM picrotoxin, 50 µM DL-aminophos-phonovalerate, and 1 µM tetrodotoxin. Verification that mEPSCs were mediated by AMPARs was achieved by adding 50 µM CNQX at the end of recordings. Recordings were filtered at 5 kHz and digitized at 20 kHz. The data were low pass-filtered using a 1 kHz cut-off and analyzed blind to condition with Mini-Analysis software (Synaptosoft).

Slice immunohistochemistry

Adult mice were perfused as described in Srivastava et al. 2012. 75 µm thick slices were sectioned and immunostained as described in Hedrick and Waters, 2010, with primary antibodies to ankyrin-G (Santa Cruz) and bassoon (Assign Technologies).

FRAP

Cortical neurons for FRAP experiments were grown on glass bottom culture dishes (MatTek) and transfected with GluA1-SEP alone, or GluA1-SEP and mcherryAnkG190 as described above. Neurons were imaged with an Andor spinning disc confocal microscope (NU Nikon Cell Imaging Facility) in an OKO labs stage CO_2 incubator. Images were captured with an EMCCD camera of 512x512 pixel resolution every 2s for 40s and then every 20s for 200s. 100% laser power pulses of 1ms (2 iterations) were used to bleach GluA1-SEP clusters. Fluorescence intensity of bleached GluA1-SEP clusters was measured and normalized to the fluorescence of an unbleached region to correct for photobleaching. These values were normalized to the mean of the 5 frames prior to bleaching, and the lowest value in the dataset was subtracted from all values. Recovery data points were then fitted to a one-phase association exponential in GraphPad Prism. The mobile fraction was calculated as an average of the plateaued fluorescence level and expressed as a percentage of the pre-bleached level.

Coimmunoprecipitation assays

Coimmunoprecipitation assays were performed as in Copits and Swanson, 2013 with modifications. Briefly, adult rat cortex was dissected and homogenized in pull-down buffer (50 mM HEPES pH 7.5, 1 % triton X-100, 150 mM NaCl, 1 mM EDTA, 1mM AEBSF with protease inhibitor cocktail (Roche) and phosphatase inhibitor (Sigma)) and solubilized for 1 hour at 4°C. Solubilized material was centrifuged at 20,000 g for 25 minutes at 4°C and the supernatant was precleared with protein A/G beads for 1 hour. Proteins were immunoprecipitated with 3 µg of antibody overnight at 4°C, followed by a 1 hour incubation with protein A/G beads. Beads were then washed extensively and bound complexes were analysed by SDS-PAGE and western blotting.

Fear conditioning and fractionation

All procedures were approved by Northwestern University's Animal Care and Use Committee, and are in compliance with National Institutes of Health standards. Nine-week old C57Bl/6N mice (Harlan; n = 5) were placed in a clean Plexiglas chamber (35x20x20 cm), with a stainless steel rod floor (4 mm diameter, 0.9 cm center to center), inside a sound attenuating cabinet (TSE) for a 3min exploration period, followed by a 2-sec, 0.7mA foot shock. Thirty minutes following the behavioral procedure, mice were euthanized and the hippocampus rapidly dissected and frozen over liquid nitrogen. Tissue from naïve mice, which encountered no behavioral paradigms, was collected the same day. Hippocampal tissue was processed with the Subcellular Protein Fractionation Kit for Tissue (ThermoScientific) according to manufacturer's instructions.

Synaptoneurosome preparations

Synaptoneurosome preparations were performed as in Villasana et al., 2006. Adult rat cortex was homogenized in 2 mL of synaptoneurosome buffer (10 mM HEPES, 1 mM EDTA, 2 mM EGTA, 100 mM AEBSF, Roche Complete ULTRA Tablets, Sigma Seronie/Threonine Phosphatase inhibitors #3, pH 7.0). The homogenate was then sonicated (3 pulses, power of 1) using a Sonic dismembrator (Fisher Scientific) and sample was set aside as the homogenate fraction. The remaining sample was filtered twice through three layers of a pre-wetted 100 µm pore nylon filter (Millipore) held in a Swinnex® 25 filter holder, followed by filtration through a pre-wetted 5 µm pore hydrophilic filter (Millipore) held in a Swinnex® 13 filter holder. The final filtrate was centrifuged at 1,000 g for 10 minutes. The pellet was resuspended in 200 uL RIPA buffer, agitated for 40 minutes, and spun down at 16,000 g for 10 minutes. The

supernatant was isolated as the synaptoneurosome fraction. After performing a BCA assay, 7.5 ug of each fraction was analysed by SDS-PAGE and western blotting.

Supplemental Movie Legend

Movie S1

3D-reconstruction of dendritic spine shown in Figure 2H,I. SIM reveals spine structure as determined by GFP-filled neuron (green). Removal of the green channel enables visualization of PSD95 in spine head (blue) which is surrounded by 3 ankyrin-G nanodomains (red).

Supplemental References

Amatrudo, J.M., Weaver, C.M., Crimins, J.L., Hof, P.R., Rosene, D.L., and Luebke, J.I.(2012). Influence of highly distinctive structural properties on the excitability of pyramidal neurons in monkey visual and prefrontal cortices. In Journal of Neuroscience, pp13644-13660.

Copits, B.A. and Swanson, G.T. (2013). Kainate receptor post-tanslational modifications differentially regulate association with 4.1N to control activity-dependent endocytosis. In JBC, pp. 8952-8965.

Hedrick, T., and Waters, J. (2010). Physiological properties of cholinergic and non-cholinergic magnocellular neurons in acute slices from adult mouse nucleus basalis. PloS one 5, e11046.

Srivastava, D.P., Jones, K.A., Woolfrey, K.M., Burgdorf, J., Russell, T.A., Kalmbach, A., Lee, H., Yang, C., Bradberry, M.M., Wokosin, D.*, et al.* (2012). Social, communication, and cortical structural impairments in Epac2-deficient mice. The Journal of neuroscience : the official journal of the Society for Neuroscience 32, 11864-11878.

Woolfrey, K.M., Srivastava, D.P., Photowala, H., Yamashita, M., Barbolina, M.V., Cahill, M.E., Xie, Z., Jones, K.A., Quilliam, L.A., Prakriya, M., and Penzes, P. (2009). Epac2 induces synapse remodeling and depression and its disease-associated forms alter spines. In Nat Neurosci, pp. 1275-1284.

Villasana, L.E., Klann, E., Tejada-Simon, M.V. (2006). Rapid isolation of synaptoneurosomes and postsynaptic densities from adult mouse hippocampus. In J Neurosci Methods, pp 30-36.